ISSN (p) 0321-2211, ISSN (e) 2663-3450

НАУКОВІ ТА ПРАКТИЧНІ ПРОБЛЕМИ ВИРОБНИЦТВА ПРИЛАДІВ ТА СИСТЕМ

DOI: 10.20535/1970.70(2).2025.348001
UDC 621.382

AMPLITUDE-STABILIZED HARMONIC CURRENT SOURCE FOR MEMS MICROHEATERS WITH GROUNDED LOAD

Hrebonkin Ye. O.
National Technical University of Ukraine "Igor Sikorsky Kyiv Polytechnic Institute"
Kyiv, Ukraine
E-mail: ye.hrebonkin-me28@lll.kpi.ua

This paper presents the design, development, and experimental validation of a multi-stage AC current source with amplitude stabilization, specifically created for MEMS microheaters with grounded load in 3-omega gas sensing applications. The proposed system is based on a Raspberry Pi Pico microcontroller, an external R-2R ladder digital-to-analog converter, cascaded inverting amplifier stages, and an improved Howland current pump that ensures precise stabilization of the excitation current amplitude. Such an approach enables generation of a spectrally clean sinusoidal signal in the 20 Hz–20 kHz frequency range, with adjustable current amplitude up to 5 mA, zero-level offset control, and stable operation across heater-resistor systems with impedances from 50 Ω to 3 kΩ. Compared with conventional voltage-driven circuits, current-driven excitation in the 3-omega method ensures higher reproducibility, improved calibration consistency, and more accurate interpretation of thermal responses. The developed device successfully addresses challenges associated with grounded heater configurations and reduces dependence on bulky laboratory-grade instruments, offering a compact and low-cost solution suitable for both fixed-frequency and broadband thermal characterization of gases.

Experimental results demonstrate that the source maintains frequency stability above 99.9 % and total harmonic distortion below 1 %, while deviations in current amplitude across the supported load range remain within acceptable limits (<1%), ensuring reliable application in thermal property extraction. The significance of the work lies not only in the practical realization of a robust excitation source but also in its potential to support integration of MEMS thermal gas sensors into portable and embedded platforms. The modular design and firmware-controlled signal generation enable straightforward tuning and future improvements such as digital feedback, precision matched resistor networks, or single-supply architectures.

Overall, the developed current source provides a valuable and adaptable tool for experimental gas analysis, representing a meaningful step toward miniaturized and accessible gas sensing systems..

Keywords: *3-omega method, thermal gas sensing, MEMS microheater, AC current source, current stabilization.*

Introduction. Problem Statement.

Gas analysis constitutes a critical component of environmental monitoring, enabling the timely detection of atmospheric composition changes resulting from both natural processes and anthropogenic activities. Accurate measurement of greenhouse gases, volatile organic compounds (VOCs), carbon monoxide, nitrogen and sulfur oxides is essential for assessing air quality, predicting climate dynamics, and implementing effective strategies to mitigate ecological risks. Modern analytical techniques—particularly those leveraging MEMS-based technologies—facilitate highly sensitive, rapid detection under challenging environmental conditions, making them indispensable in domains such as environmental surveillance, industrial safety, and urban air quality assessment. Recent studies indicate that the global gas sensor market is experiencing sustained growth, fueled by stricter environmental regulations and ongoing innovations in sensing technologies [1].

Among the various strategies for gas identification, the measurement of thermophysical parameters–most notably thermal conductivity–represents a robust and informative approach [2]. MEMS microheaters [3] are commonly used in such measurements, offering localized thermal excitation and sensitive detection of resistance or temperature variations induced by gas interactions.

Thermal conductivity measurement techniques are broadly categorized into steady-state and transient methods [4]. Transient approaches are particularly advantageous due to their reduced dependence on initial thermal conditions and their ability to yield results more rapidly than steady-state techniques, which require thermal equilibrium to be established [4]. Moreover, when implemented in the frequency domain, transient techniques benefit from the

suppression of DC drift and contact resistance effects via narrowband harmonic filtering [5]. These characteristics necessitate strict requirements for spectral purity and amplitude stability of the excitation signal.

Within this context, the 3-omega (3ω) method emerges as a paradigmatic frequency-domain transient technique. A sinusoidal current applied to a resistive microheater induces periodic Joule heating at twice the excitation frequency. This in turn modulates the heater's temperature, resulting in a time-varying resistance that generates a voltage response containing a third-harmonic component. The amplitude and phase shift of such 3ω signal are governed by the thermal impedance of the surrounding medium, providing a basis for the quantitative characterization of gas thermal properties [6]. The method enables broadband thermal analysis with high immunity to environmental noise, rendering it highly suitable for gas sensing applications [4].

In 3ω-based gas sensing, current excitation is generally preferred over voltage excitation due to its more direct and reproducible relationship between the input electrical parameter and the resulting thermal power. Under constant-current operation, the current amplitude remains fixed, while the resistance of the heater varies predictably with temperature. This modulation directly affects the dissipated power—proportional to the product of resistance and the square of the current—thereby generating the third-harmonic voltage component. Crucially, current-driven operation should not be conflated with constant-power excitation: although power varies, its modulation is governed solely by the thermal response of the system, yielding a predictable dependence of the 3ω signal on the applied current [4]. In contrast, voltage-driven excitation introduces a reciprocal dependence of power on instantaneous resistance, which complicates interpretation due to nonlinear mixing, increased sensitivity to the source impedance, and elevated measurement uncertainty. Current excitation thus offers improved calibration consistency, reproducibility, and model accuracy—factors essential for reliable extraction of gas thermal properties.

Despite its methodological advantages, practical implementation of the 3ω method remains constrained by the limitations of conventional signal generation circuits, which typically stabilize voltage rather than current. Moreover, the widespread use of grounded loads in experimental configurations further complicates the application of standard current-source architectures. These characteristics make the proposed current source well-suited for integration into experimental setups aimed at high-precision thermal characterization of gaseous media, where accurate and stable thermal excitation of the microheater is required.

State-of-the-Art Overview. Recent developments in low-power analog front ends, portable impedance analyzers, and gas sensing instrumentation have introduced various strategies for generating sinusoidal excitation signals and current sources. However, many existing designs are either targeted toward ultra-low-power biomedical use [7], or require custom integrated circuitry [8], making them impractical or overcomplicated for MEMS-based thermal gas sensor applications, where moderate frequency and current ranges are required.

In particular, systems described in [7] focus heavily on frequency agility and signal linearity, often implementing complex feedback-based or DDS-based solutions. While these platforms offer wideband control and precision (e.g., THD < 0.2 %), they require significant hardware complexity and are typically unsuitable for generating several milliamps of current into kilohm-range loads. Similarly, the current excitation circuits described in [9] rely on multi-stage feedback loops and integrated active filtering, requiring precise matching and component tuning.

Older solutions such as [10] rely on phase-locked loop techniques and analog oscillators, which limit flexibility and frequency control granularity. Designs like [11] and [12] describe general-purpose sinewave generation and power delivery systems, but omit fine control of current amplitude stabilization, which is critical in 3-omega-style measurements. Furthermore, most of these approaches do not support grounded load configurations — a requirement for some of MEMS heater platforms.

The device presented in this work addresses several of the above limitations. It provides stable, adjustable, bipolar AC current excitation in the range of 0-5 mA across resistive loads from 50 Ω to 3 kΩ, supporting excitation frequencies from 20 Hz to 20 kHz with high output symmetry. While the sinewave generated via an 8-bit R-2R DAC does introduce stepwise quantization, the resulting staircase waveform (with steps of ~30 mV at ±1.4 V peak) is thermally smoothed by the heat capacity of the heater and gas medium, making it effectively indistinguishable for thermal analysis purposes. Unlike more complex solutions, this design is based entirely on accessible discrete components (Raspberry Pi Pico, LM741/LM358 op-amps, and discrete resistors), without the need for custom silicon or high-speed ADCs.

Importantly, the improved Howland Current Pump architecture used here ensures low output impedance and stable current amplitude delivery into grounded loads – a configuration not supported in most prior works [13]. Additionally, the modular nature of the implementation enables frequency and amplitude tuning via firmware and trimmer resistors, allowing compensation of amplitude drift due to capacitive filtering (as discussed in the corresponding evaluation section). Compared to the bulky or cost-intensive designs in [7] and [8], the

proposed system represents a practical and adaptable approach to current delivery for thermal gas sensing MEMS-heater applications.

Objective. The objective of this study is the development and experimental validation of a multi-stage circuit for generating an amplitude-stabilized harmonic alternating current, specifically designed for grounded microheaters. The proposed circuit is based on a Raspberry Pi Pico microcontroller, an external digital-to-analog converter (DAC), inverting amplifier stages built using LM741 and LM358 operational amplifiers, and an improved Howland current pump that ensures precise current stabilization. This design enables the generation of a spectrally pure enough harmonic signal over a wide frequency range with stable current amplitude, along with the ability to adjust the amplitude setpoint of the stabilized current as well as the zero-offset level. These features make the system suitable for high-precision experimental determination of the thermal properties of gaseous media for further gas characterization.

Design Considerations

The development of the presented amplitude-stabilized AC current source for microheaters with grounded load was guided by the design requirements presented in Table 1 below.

Table 1. Initial requirements for the proposed device

Parameter	Specification
Supported load resistance (heater + series resistor)	50 Ω – 3 kΩ
Output current amplitude range (at specified loads)	0 – 5 mA (user-adjustable)
Output frequency range	20 Hz – 20 kHz
Frequency stability	>99.9%
Total harmonic distortion (THD)	<1%
Output signal symmetry	Bipolar signal with adjustable zero-level offset
Load reference connection	Grounded (common with system ground)

Based on the requirements listed in Table 1, a modular circuit architecture was developed. The subsequent section presents the complete schematic and outlines the function and configuration of each constituent stage.

Circuit Diagram and Component Description

The proposed circuit (Figure 1) comprises three main stages.

The first stage generates a zero-crossing harmonic signal at the defined frequency.

The second stage includes two inverting operational amplifiers designed to increase the voltage amplitude of the sine wave while preserving its phase.

The third stage is an Improved Howland Current Pump [9], which functions as a current amplitude stabilizer. Each of these stages is discussed in detail later in the manuscript.

First stage – the zero-crossing sine wave generator of a software-defined frequency

The first stage (Figure 2) consists of a Raspberry Pi Pico microcontroller programmed with the custom firmware, an R-2R external DAC and the decoupling capacitor to remove the DC component of the output signal.

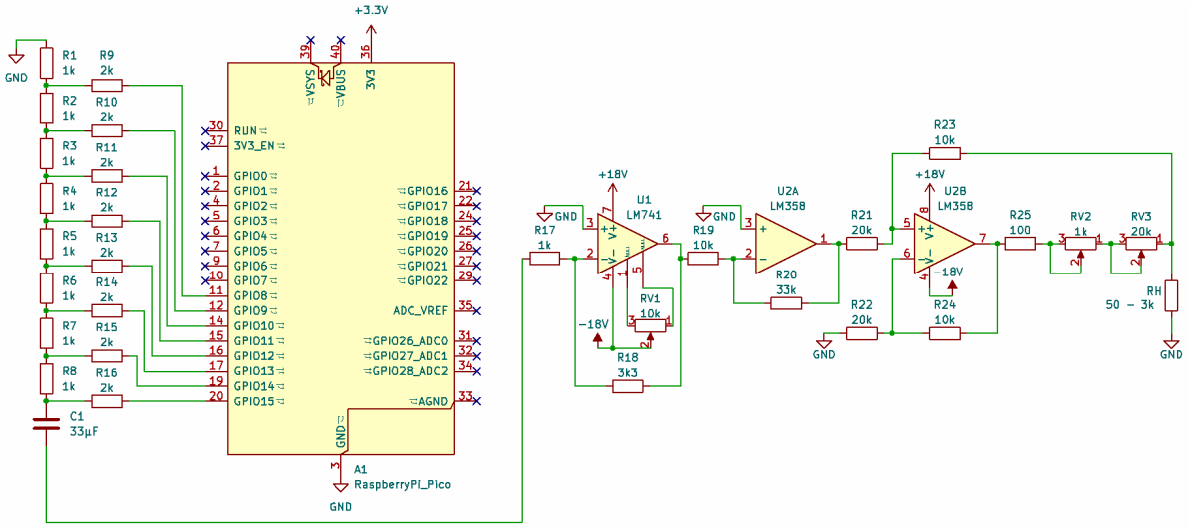

Fig. 1. Schematic diagram of the proposed current source

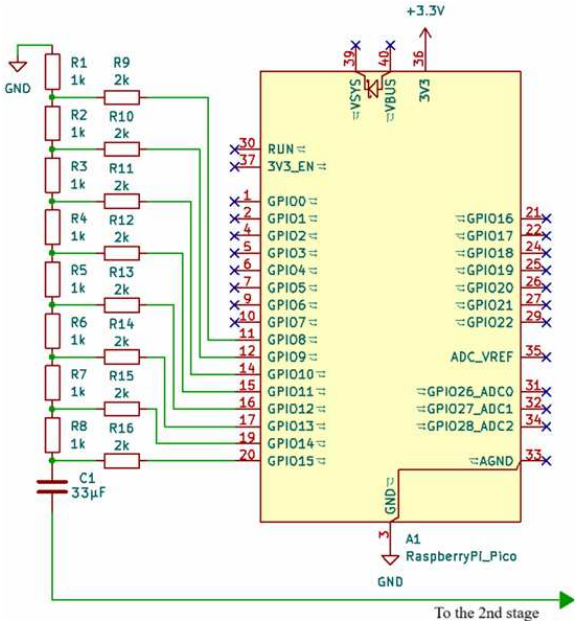

Fig. 2. The first stage of the proposed schematics

The Raspberry Pi Pico is used as a programmable digital sine wave generator by leveraging its dedicated programmable input/output (PIO) subsystem in combination with a dual-channel direct memory access (DMA) controller.

This architecture allows waveform data, pre-computed and stored in memory, to be streamed directly to the output pins with strict timing control and without continuous intervention from the CPU. As a result, the Pico can operate reliably as a compact and cost-efficient arbitrary waveform generator.

The sinusoidal waveform is represented digitally by a lookup table stored in a buffer of 4096 samples. Each entry is computed as a scaled value of the sine function, fitted to the 8-bit output resolution of the device. This high buffer depth ensures that the waveform maintains good fidelity even at relatively low frequencies, where the effective number of samples per period becomes especially important for minimizing harmonic distortion. By defining multiple complete sinusoidal cycles within the buffer, the system can adjust the ratio of buffer size to cycle length in order to control the playback frequency.

The actual output frequency is governed by three parameters: the clock frequency of the PIO state machine, the total number of samples in the buffer, and the number of sinusoidal cycles contained within that buffer. When generating signals in the higher frequency range (above approximately 1.8 MHz), the system increases the number of cycles encoded in the buffer in order to match the desired output frequency at the fixed PIO clock rate. For lower frequency ranges, by contrast, the PIO clock frequency itself is adjusted, thereby slowing down the playback rate of the buffer contents without the need to recalculate the sinusoidal samples. This dual mechanism of frequency adjustment provides a flexible way to span a broad operating range, covering frequencies from a few tens of hertz to several megahertz, while maintaining stable waveform reproduction.

A critical aspect of the implementation is the elimination of discontinuities during waveform playback. To achieve this, the Pico employs a ping-pong DMA configuration, in which two DMA channels alternately supply the PIO transmit FIFO with blocks of waveform data. While one channel is actively transferring data, the other is automatically reloaded and prepared for the next transfer cycle. This seamless handover between DMA channels guarantees that the sinusoidal signal remains continuous and free of glitches even when operating at high update rates.

This digital bitstream is then converted into an analog voltage waveform by an external digital-to-analog converter (DAC) based on an R-2R resistor ladder network. In this scheme, the eight parallel output pins of the Pico deliver the 8-bit waveform samples directly to the ladder, which reconstructs the discrete values into a continuous sinusoidal voltage. The design choice was made between two well-known resistor-based DAC architectures: the Weighted Resistor Network and the R-2R Ladder Network. A comparative analysis favored the R-2R configuration, primarily due to its requirement for only two resistor values (1 kΩ and 2 kΩ), which are easier to source and match precisely [14]. In contrast, the Weighted Resistor Network demands eight distinct, precisely matched resistor values — one for each bit — despite requiring fewer components overall [15] (8 resistors versus 16 in the R-2R design). Given the trade-off between component count and ease of implementation with standard resistor values, the R-2R topology was selected as the more practical solution for this application. Typically, resistor values in such R-2R ladder designs range from 1 kΩ to 10 kΩ for *R*, with *2R* being exactly twice that value.

Taking into account the input impedance of the subsequent amplifier stage as well as the output characteristics of the Raspberry Pi Pico GPIO pins, resistor values of R = 1 kΩ and $2R$ = 2 kΩ were selected for this implementation. In such configuration, the sine waveform is composed of small discrete steps due to DAC quantization (Figure 3). However, with a step size of approximately 30 mV and a full-scale amplitude of ±1.4 V, this discretization is negligible in practice. The small voltage transitions are effectively smoothed out by the thermal inertia of the microheater and the surrounding gas environment, resulting in continuous thermal excitation.

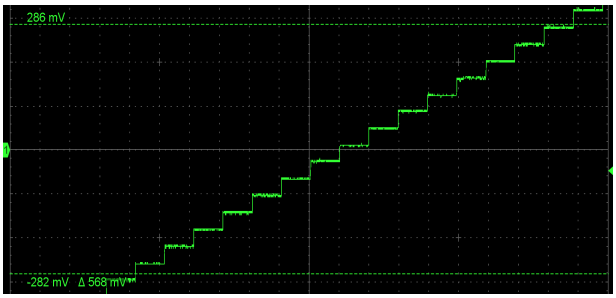

Fig. 3. Oscilloscope trace of discrete steps due to DAC quantization

The coupling capacitor, placed directly after the R–2R ladder DAC, does not only serve to remove the DC component of the digitally synthesized waveform but also forms a high-pass filter together with the effective resistance seen at its terminals. This effective resistance is the sum of the equivalent output resistance of the R–2R network and the input resistance of the following amplifier stage. As a result, the overall transfer function of this stage can be described as that of a first-order high-pass filter with the cutoff frequency [16]:

$$f_C = \frac{1}{2\pi R_{eff} C} \quad (1)$$

where C is the capacitance of the coupling capacitor and $R_{eff} = R_{out} + R_{in}$, with R_{out} being the output equivalent resistance of the R–2R ladder and R_{in} the input resistance of the subsequent operational amplifier stage.

The frequency response of this filter follows the standard form [17]:

$$\left|H(f)\right| = \frac{\omega R_{eff} C}{\sqrt{1 + (\omega R_{eff} C)^2}}$$

with ω = 2πf.

At frequencies much higher than f_c, the capacitor effectively acts as a short circuit for the AC component, and the output voltage amplitude approaches the input amplitude. At frequencies near or below f_c, however, the amplitude is attenuated, which results in the observed deviation of the sinusoidal output amplitude at low frequencies. The value of the coupling capacitor was chosen as C=33 μF in order to satisfy two opposing design constraints. On the one hand, the cutoff frequency of the high-pass network formed with the effective resistance at the DAC output must be sufficiently low so that the sinusoidal excitation in the intended operating band (tens of hertz to several kilohertz) is not attenuated. From the equation (1), it becomes obvious that a larger capacitance value shifts the cutoff frequency downward and reduces amplitude drop at the lower edge of the spectrum. On the other hand, excessively large capacitance at the DAC output would present a heavy reactive load to the preceding stage, thereby increasing transient currents during waveform transitions and potentially distorting the synthesized waveform. The chosen value of 33 μF represents a practical compromise and is compliant with E24 series of preferred numbers: it lowers the cutoff frequency well below the minimum frequency of interest, thereby ensuring negligible attenuation (<1%) even in the sub-tens-of-hertz range, while at the same time keeping the reactive loading of the R–2R ladder and the operational amplifier input within acceptable limits. This selection thus guarantees both fidelity of the AC coupling and stable operation of the preceding digital-to-analog conversion stage.

The output of the first stage is an AC sine wave with a frequency defined by the Raspberry Pi Pico firmware. The corresponding oscilloscope trace of this stage's output is shown in Figure 4.

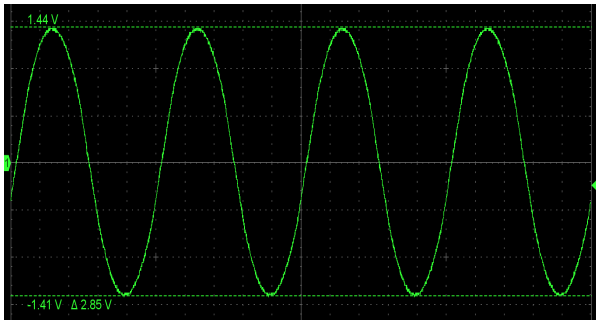

Fig. 4. Oscilloscope trace of the 1st stage's output configured at 20Hz

Second Stage – Voltage Amplification and Zero-Level Offset Adjustment

In practice, the second stage of the discussed circuitry consists of two successive operational amplifier sub-stages (Figure 5). However, in the present description they are considered as a single functional block, since both sub-stages perform identical operations in terms of their role in the signal chain.

The choice of this topology was dictated by the requirement that the output signal must remain non-inverted with respect to the digitally generated reference signal. To satisfy this constraint while simultaneously providing the necessary voltage gain, two inverting amplifier configurations were cascaded, resulting in an overall non-inverting transfer

characteristic.

The first sub-stage is built around an LM741 operational amplifier, selected primarily due to its availability, low cost, and sufficient performance within the target frequency range specified for the system [18]. This stage also incorporates a trimming network, which allows adjustment of the output offset to eliminate residual DC components in the signal. This arrangement enables fine compensation of residual DC components that may remain after digital-to-analog conversion, ensuring that the amplified output waveform is centered precisely around zero volts. Such trimming is particularly important for subsequent stages, as even a small offset at the input leads to asymmetric drive conditions and distortion of the heating current in the MEMS heating element. By providing stable zero-offset control, the circuit maintains the symmetry of the sinusoidal excitation and improves the accuracy of thermal response measurements. The corresponding oscilloscope trace of this sub-stage's output is shown in Figure 6. The signal exhibits a 180° phase shift, which corresponds to the inverting amplification characteristic of this sub-stage.

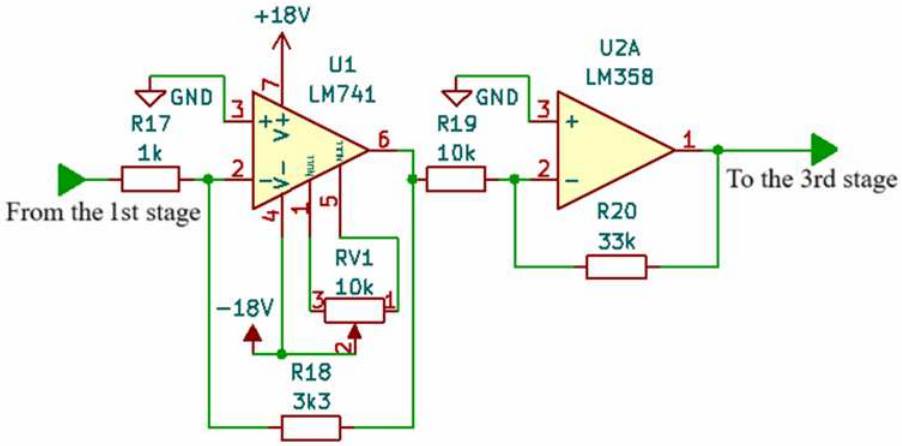

Fig. 5. The second stage of the proposed schematic

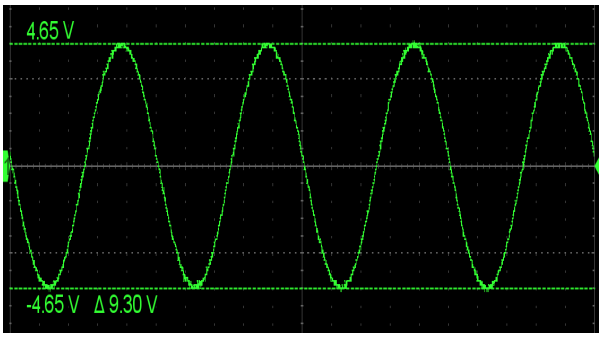

Fig. 6. Oscilloscope trace of the output from the first inverting amplifier in the second stage of the proposed circuit

The second sub-stage, implemented on one half of the LM358, performs the same inverting amplification as the first, but without the need for an offset control network. Its sole function is to provide an additional gain of –3.3, so that in combination with the first amplifier the overall block achieves the required non-inverted x10.89 voltage gain.

The use of inverting amplifier configurations with negative feedback was deliberate. Compared to positive-feedback schemes, negative-feedback amplifiers provide higher linearity, greater stability against component tolerances, and predictable gain determined solely by resistor ratios [19]. These features are particularly important in precision measurement systems such as the present one. The trade-off, however, lies in the reduced open-loop bandwidth utilization and the introduction of inversion, which in this case is compensated by cascading two identical inverting stages.

The resistor values were chosen with consideration of both impedances matching between the preceding DAC stage and the subsequent current-drive stage, and the desired gain factor. The choice of resistor values differs between the two sub-stages: in the LM741 circuit, relatively low values of 1 kΩ and 3.3 kΩ were adopted to ensure proper impedance matching with the output of the preceding R-2R ladder DAC, whose drive capability is limited and thus benefits from a lower input resistance at the following stage. In contrast, the LM358 stage employs larger resistor values of 10 kΩ and 33 kΩ. This reduces the current drawn from the output of the first amplifier, minimizes unnecessary power dissipation, and helps to avoid loading effects while still preserving the precise gain ratio defined by the resistor pair. In this way, each stage is optimized with respect to both the electrical characteristics of the component it interfaces with and the overall requirements of the signal chain. Each inverting amplifier is configured with a gain of –3.3, producing a total gain of +10.89 at the block output. Given that the maximum output of the Raspberry Pi Pico is limited to 3.3 V, the removal of the DC offset in addition of other losses yields a symmetrical input signal of approximately ±1.4 V, as shown in Figure 4. After amplification by a factor of 10.89, the resulting signal amplitude reaches approximately ±15.25 V. This voltage level was

selected to satisfy two constraints: first, to ensure that sufficient power can be dissipated in potential heater elements under test, and second, to accommodate the limitations of the subsequent improved Howland current pump stage. The latter tends to lose stability when its output voltage amplitude approaches that of the driving input signal, thus necessitating the use of a higher-amplitude excitation voltage at this stage.

The output of the second stage is an AC sinusoidal waveform that preserves the frequency and phase defined by the Raspberry Pi Pico software, while its amplitude is increased to approximately ±15.25 V peak-to-peak. The corresponding oscilloscope trace of this stage's output is shown in Figure 7 below.

The signal undergoes another 180° phase shift, thereby restoring its original phase.

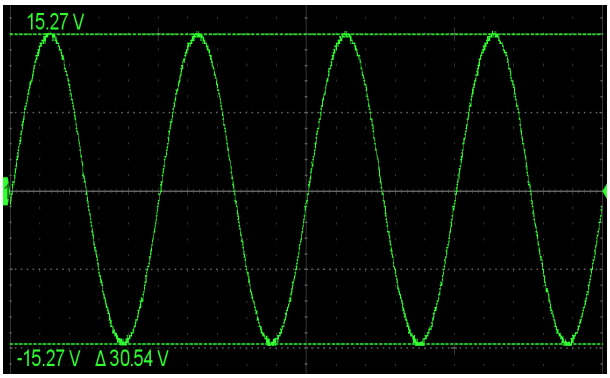

Fig. 7. Oscilloscope trace of the 2nd stage's output configured at 20Hz

Third Stage – Current amplitude stabilization using the improved Howland current pump circuit

The final stage of the excitation circuit is implemented as an *Improved Howland Current Pump (IHCP),* which serves as a voltage-controlled current source for driving the MEMS heater (RH in the Fig. 8).

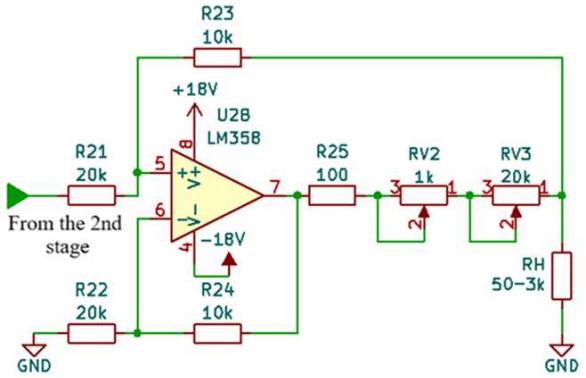

Fig. 8. The third stage of the proposed schematic

The principle of this circuit lies in the precise balancing of a differential amplifier configuration, in which the operational amplifier enforces a voltage across a current-sensing resistor, thereby regulating the current delivered to the load.

In the ideal case, when all resistors are perfectly matched, the output current is directly proportional to the input voltage and remains independent of the heater resistance. This makes the IHCP a suitable choice for applications requiring a stable sinusoidal current, as in the present method implementation [13]. The oscilloscope trace of the device output at 20 Hz with the current stabilized at 1.33 mA for a 1.5 kΩ load is shown in Figure 9.

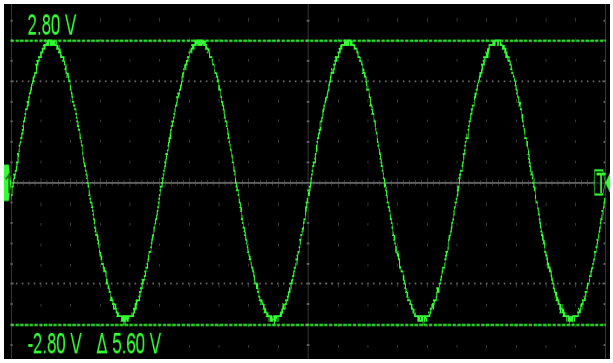

Fig. 9. Oscilloscope trace of the device output at 20 Hz with the current stabilized at 1.33 mA for a 1.5 kΩ load

In the Improved Howland Current Pump, the amplitude of the stabilized output current is determined primarily by the current-sense resistor placed at the output branch of the operational amplifier. The theoretical relationship between the input voltage and the load current is expressed as:

$$I_H = -\frac{R_{24}}{R_{23}R_S}V_{in},$$

where I_H is the current through the heater, V_{in} is the driving sinusoidal voltage provided by the preceding amplification stages, R_{23} and R_{24} are corresponding resistors from the schematic diagram (see Figure 8), R_s is the effective value of the sense resistor which consists of R25, RV2 and RV3 resistors connected in series [13].

In the present design, this element is implemented as a composite network consisting of a fixed resistor R25 in series with two variable resistors RV2 (coarse adjustment) RV3 (fine adjustment). Furthermore, the inclusion of the fixed element (R25) ensures that the total resistance cannot be reduced to zero, thereby protecting the operational amplifier from user error during setting. The practical role of the variable resistors (RV2 and RV3) is to tune the maximum output current delivered to the heater, effectively setting the amplitude of the excitation.

The advantages of the Improved Howland Current Pump include its ability to source or sink current, its inherently high output impedance, and the possibility of achieving precise control of load current using a single operational amplifier stage [9]. These features allow the circuit to maintain constant excitation conditions even under variations in heater resistance, which may occur due to temperature-

dependent changes during operation. Nevertheless, the circuit also exhibits well-documented limitations. Its accuracy is strongly dependent on resistor matching, and even small mismatches can introduce error into the regulated current. In addition, the IHCP is constrained by the compliance voltage of the operational amplifier; in practice, it ceases to function correctly once the required output voltage exceeds the available input headroom [11]. This limitation explains the necessity of the preceding amplification stages, which elevate the driving signal to levels sufficient for maintaining stable current delivery within the voltage range permitted by the IHCP.

Compared with alternative current source topologies such as Wilson mirrors, op-amp/transistor source circuits, or floating-load drivers, the IHCP was selected for its wide load compliance range, and the ease with which its performance can be tuned using precision resistors. While these benefits come at the expense of sensitivity to resistor tolerances and limited voltage compliance, the IHCP provides a favorable compromise between simplicity, adjustability, and performance, making it particularly well suited to the present application.

Evaluation of Compliance with Design Requirements

Design-Specified Parameters Without Experimental Validation

A number of target parameters defined in the design requirements (Table 1) are inherently ensured through the circuit topology and component selection. Their compliance does not require separate experimental verification, as they are determined by theoretical considerations and guaranteed by the characteristics of the selected components.

Maximum Output Current. The maximum output current was defined as 5 mA. This value is motivated by the typical power consumption of microheater-based sensing structures, which generally operate within a 10-20 mW power range. For instance, a representative configuration consisting of two 1 kΩ heater segments in parallel or series (depending on the application) [20] results in a total resistance of ~2 kΩ. Driving such a load with 5 mA yields a power dissipation of 50 mW, providing a safe margin above the typical operating point while remaining within the limits of standard MEMS heater design constraints.

Maximum Output Voltage. The maximum output voltage of ±15 V is dictated by the upper bound of the supported load resistance (3 kΩ), which accounts for a typical configuration comprising two 1 kΩ heater segments and an additional 1 kΩ series resistor typically used for current measurements. According to Ohm's law, supplying 5 mA across 3 kΩ requires 15 V. This voltage range is readily achievable within the selected architecture, as described in the section about the second stage of the proposed schematic, where each inverting amplifier stage provides a gain of −3.3. Given the DAC output swing of ±1.4 V, the overall gain results in a maximum amplitude of approximately ±15.25 V, well within the output range of the chosen operational amplifiers. The op-amps are powered by a dual ±18 V supply, ensuring sufficient headroom to support this output swing without distortion.

Supported Load Resistance Range. The supported load resistance range of 50 Ω to 3 kΩ reflects the expected electrical characteristics of typical MEMS microheaters and their associated series resistors. This range is compatible with the output impedance characteristics of the final current source stage - an improved Howland current pump - as well as the drive capabilities of the selected op-amps in the configuration used.

Maximum Output Frequency. The upper frequency limit of 20 kHz is well within the capabilities of both the Raspberry Pi Pico and the selected op-amps. The microcontroller supports fast PWM and high-speed DAC emulation, while the op-amps used (LM741, LM358) operate comfortably within this frequency range for the required signal amplitudes and load conditions. As such, no experimental verification of this parameter is required; however, the frequency response characteristics over the 20 Hz to 20 kHz range will be measured and presented in the following sections.

Output Signal Symmetry. The output signal is designed to be symmetric with respect to the system ground. A zero-level offset adjustment is included in the second amplifier stage using the LM741, allowing fine-tuning of the DC level to ensure equal positive and negative half-cycle amplitudes. This satisfies the design requirement of producing a bipolar, zero-centered sine wave.

Load Reference Grounding. The circuit is explicitly designed to support grounded loads. The Howland current source topology and the use of inverting amplifier stages ensure that the reference (zero) potential of the heater is shared with the system ground. This feature allows the circuit to be integrated seamlessly with grounded measurement equipment and systems without introducing floating nodes or ground loops.

Frequency Response

The frequency response was measured across the range of 20 Hz to 20 kHz. A 1.5 kΩ resistive load was used, and the current amplitude was stabilized at 2.67 mA, corresponding to a voltage amplitude of 4 V across the load at 20 Hz. The resulting frequency response plot is presented in Figure 10.

As shown in Figure 10, the current amplitude exhibits a rising trend in the low-frequency range from 20 Hz to approximately 200 Hz. Beyond this point, the frequency response flattens, and amplitude stabilization remains nearly constant across the full upper frequency range.

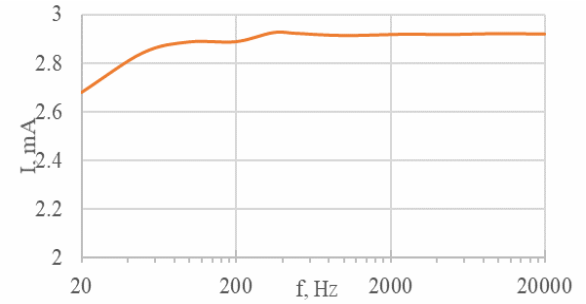

Fig. 10. Frequency response of the proposed device across the range of 20 Hz to 20 kHz

This behavior is characteristic of a high-pass filter and is attributed to the presence of the DC-blocking capacitor placed at the output of the first stage. In this design, a 33 µF electrolytic capacitor was used.

Unfortunately, increasing the capacitance further to reduce low-frequency attenuation would lead to undesirable side effects, as discussed in the corresponding design section. Nevertheless, several practical approaches can be considered to address this limitation:

- Fixed-frequency operation: If the gas sensor is intended to operate at a single frequency, the non-uniformity of the response at lower frequencies becomes irrelevant.
- Manual amplitude adjustment: In applications requiring measurements at multiple discrete frequencies, the current amplitude can be manually re-adjusted between measurements using trimmer potentiometers RV2 and RV3.
- High-frequency-only range: If the sensing application targets frequencies above 200 Hz, the effect can be safely neglected.
- Software-based compensation: The frequency response can also be equalized programmatically. Since the attenuation caused by the coupling capacitor is predictable and consistent, the output amplitude of the waveform generated by the Raspberry Pi Pico can be pre-compensated for each frequency. This allows the system to restore the flatness of the frequency response and maintain constant current excitation across the full operational range.

Moreover, an analysis of the frequency dependence of the voltage gains in the subsequent amplifier stages revealed no measurable variation across the full frequency range. As a result, these stages do not contribute to the shape of the frequency response, and their effect can be considered frequency-independent.

Frequency Setting Resolution and Stability

The resolution of the output frequency is defined by the firmware running on the Raspberry Pi Pico. Although, the “float” variable type allows to set the number with 7-digits preciseness, the achievable frequency setting resolution is mainly determined by the waveform buffer length and the number of cycles per buffer. This level of precision is sufficient for all target applications and is guaranteed by the waveform generation algorithm implemented in the Raspberry Pi Pico firmware.

The measurements were performed using National Instruments LabVIEW software in conjunction with a National Instruments USB-6009 DAQ device [21].

The project was configured to record the input signal frequency and to store its maximum and minimum values during the measurement interval. For each frequency point, data were acquired over a 1-minute period. The results are summarized in Table 2.

Table 2. Frequency stability over a 1-minute period of measurement time

Frequency f, Hz	**f_{min}, Hz**	**f_{max}, Hz**	**$\Delta f_{max-min}$, Hz**	**$\Delta f_{max-min}$, %**
20	20,0001	20,0005	0,0004	0,002
50	50,0003	50,0012	0,0009	0,0018
100	100,001	100,002	0,001	0,001
200	200,003	200,003	0	0
500	500,007	500,008	0,001	0,0002
1000	1000,01	1000,02	0,01	0,001
5000	5000,07	5000,07	0	0
20000	20000,3	20000,4	0,1	0,0005

The measurements were limited by the precision of the experimental setup at different frequencies, as summarized in Table 2. At certain frequencies, such as 200 Hz and 5 kHz, no frequency deviation was observed during the measurement interval. The largest deviation occurred at 20 Hz, with a relative value of only 0.002 %, which is negligibly small and falls within the expected instrumentation error margins. These results demonstrate that the proposed design is highly stable with respect to frequency deviation and fully complies with the design requirement of >99.9 % stability.

Total Harmonic Distortion

The total harmonic distortion (THD) of the output signal was measured using the built-in instrument in National Instruments LabVIEW, titled Harmonic Distortion Analyzer. This tool performs automated spectral decomposition of the input

waveform by isolating the amplitudes of the fundamental frequency and its harmonic components, and calculates the ratio of their combined power to the total signal power, thus quantifying the level of harmonic distortion.

Measurements were conducted at a frequency of 1 kHz, which was chosen as a representative test point due to several practical and technical considerations. Firstly, 1 kHz lies within the linear and stable operating range of the analog signal generation and amplification chain. This ensures minimal influence of capacitive loading, bandwidth roll-off, or other frequency-dependent distortions that could affect measurement accuracy. Secondly, this frequency is sufficiently removed from low-frequency interference sources such as 50/60 Hz power line noise, thereby improving the signal-to-noise ratio of the harmonic analysis.

In addition, the selection of 1 kHz is directly constrained by the capabilities of the measurement hardware. Specifically, the National Instruments USB-6009 DAQ device used in the experimental setup imposes limitations on the maximum reliably analyzable frequency spectrum. Harmonic distortion measurements require that not only the fundamental but also its relevant harmonics fall well below the Nyquist limit imposed by the sampling frequency. Operating at 1 kHz ensures that several harmonic components can be captured and analyzed without encountering aliasing or spectral truncation, thereby maintaining the validity of the THD estimation. The corresponding measurement result is shown in Figure 11.

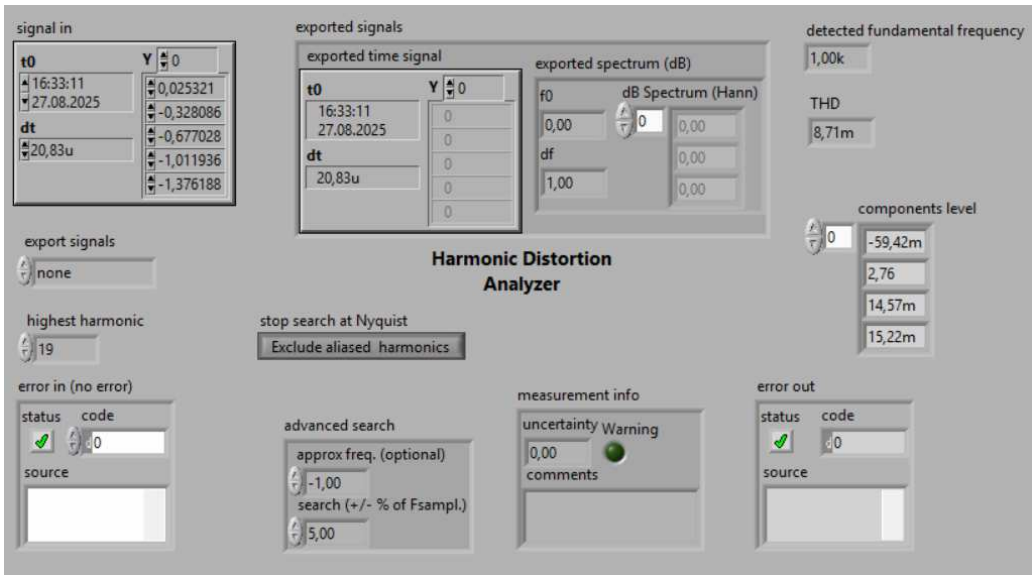

Fig. 11. The result of THD measurement at 1kHz frequency

The measured THD value at 1 kHz was 8.71 m, as reported by the Harmonic Distortion Analyzer tool in LabVIEW (see Figure 11). This corresponds to a distortion level of 0.871 %, indicating that the harmonic components contribute less than one percent of the total signal power. Such a result, with a total harmonic distortion below 1%, is fully acceptable for applications involving the measurement of thermal properties. In this context, the non-idealities introduced by the signal path - such as digital-to-analog converter quantization, reconstruction filter limitations, and amplifier nonlinearity - are effectively suppressed by the thermal inertia of the heater-environment system. As a result, these electrical distortions do not significantly influence the heating dynamics or the accuracy of resistance and temperature oscillation measurements of the microheater.

Current Amplitude Stability

To evaluate the quality of current amplitude stabilization provided by the developed source, a series of measurements were conducted using resistive loads that emulate typical microheater configurations. The tested load values were: 50 Ω, 250 Ω, 500 Ω, 1 kΩ, 1.5 kΩ, 2 kΩ, and 3 kΩ.

A reference point was established by setting the output voltage across a 3 kΩ load to exactly 4V RMS, corresponding to a target current amplitude of approximately 1.33 mA. Without modifying any circuit parameters, the load resistors were sequentially replaced with the remaining values listed above, and the resulting current amplitudes were recorded. The results of such measurements are summarized in Table 3 below, demonstrating the performance of the current source under varying load conditions.

Table 3. Performance of the presented current source under varying load conditions

R_H, Ω	V_H, V	I_H, A	I_H, mA
2980	4,001	0,001343	1,342617
1990	2,787	0,001401	1,400503
1487	2,126	0,00143	1,429724
995	1,562	0,00157	1,569849
494	0,786	0,001591	1,591093
249	0,398	0,001598	1,598394
53,4	0,0801	0,0015	1,5

The data confirms that current amplitude stabilization is successfully maintained across the entire supported resistance range, although a slight deviation is observed: on average, a shift of approximately 6 µA per 100 Ω of load change.

To estimate the potential impact of this deviation on the accuracy of thermal property measurements using the 3-omega method, consider a worst-case scenario: a nickel-based microheater with a TCR of 6×10^{-3} K^{-1} and an initial resistance of 2 kΩ, connected in series with a 1 kΩ resistor, yielding the maximum supported load of 3 kΩ.

A temperature rise of 20 °C [22] would increase the heater resistance to 2216 Ω, resulting in a current shift of around 13 µA at a stabilized current of 1.34 mA. This corresponds to a relative error of around 1 %, which is well within acceptable limits for most practical thermal gas sensing applications.

Conclusions

This work has demonstrated the design, implementation, and experimental validation of a multi-stage amplitude-stabilized harmonic current source specifically developed for MEMS microheaters with grounded loads in gas sensing applications. The proposed circuit, based on a Raspberry Pi Pico microcontroller, an external R-2R DAC, cascaded inverting amplifiers, and an improved Howland current pump, successfully meets the initial design requirements. The device provides sinusoidal excitation with amplitudes up to 5 mA across loads from 50 Ω to 3 kΩ, supporting operation over the 20 Hz–20 kHz frequency range while maintaining >99.9% frequency stability and total harmonic distortion below 1%.

The results confirm that the source ensures effective current amplitude stabilization across the supported load range, with only minor deviations (<1%) that fall within acceptable error margins for practical thermal characterization. Frequency deviation was found to be negligible, and harmonic distortion introduced by the DAC quantization, filtering, and amplifier stages is strongly suppressed by the thermal inertia of the heater–environment system, rendering the output fully suitable for 3-omega measurements.

At the same time, several limitations were identified. The low-frequency response is influenced by the coupling capacitor, leading to amplitude roll-off below ~200 Hz, which can be mitigated through manual trimming, software pre-compensation, or frequency-selective operation. The improved Howland current pump remains sensitive to resistor mismatches and compliance voltage, requiring careful manual adjustment. Additionally, the present implementation relies on dual ±18 V supply rails which limits miniaturization and integration into portable sensing platforms.

Future work should therefore focus on circuit miniaturization, integration of precision matched resistor networks, and the adoption of single-supply or rail-to-rail amplifier architectures to eliminate the need for bulky dual supplies. Firmware-based amplitude correction and the use of higher-resolution DACs may further improve spectral purity and reduce the need for manual calibration. This can be achieved by replacing the sensing resistor network with a digitally controlled high-precision resistor and incorporating a current feedback loop to the microcontroller, enabling accurate real-time current monitoring and closed-loop stabilization.

In summary, the developed current source has proven to be a low-cost, compact, and robust alternative to conventional laboratory instrumentation, fully compliant with the requirements of MEMS-heater-based thermal gas sensing.

Its demonstrated performance supports its application in experimental studies of gas thermal properties, while the identified challenges provide a clear direction for continued refinement toward practical, miniaturized sensor systems.

References

[1] S. Mor, et al., “Current Opportunities and Trends in the Gas Sensor Market: A Focus on e-Noses and Their Applications in Food Industry,” *Chemosensors*, vol. 13, no. 5, p. 181, 2025. DOI: 10.3390/chemosensors13050181

[2] Є. Гребьонкін, В. Заворотний, “Використання наноматеріалів в газових МЕМС сенсорах,” *Вчені записки Таврійського національного університету імені В.І. Вернадського, Серія:*

Технічні науки, Том 35(74), № 6, ч. 1, pp. 59–68, 2024. DOI: 10.32782/2663-5941/2024.6.1/11
[3] Є. Гребьонкін, В. Заворотний, "Мультисенсорні платформи на основі МЕМС для аналізу газів," *Перспективні технології та прилади*, Том 1, № 26, с. 38–50, 2025. DOI: 10.36910/10.36910/6775-2313-5352-2025-26-05
[4] E. L. Gardner, et al., "Micromachined thermal gas sensors - A review," *Sensors*, vol. 23. no. 2, 681, 2023. DOI: 10.3390/s23020681
[5] R. Salim, "Thermal conductivity measurements using the transient hot-wire method: a review," *Measurement Science and Technology*, vol. 33, no. 12, 125022, 2022. DOI: 10.1088/1361-6501/ac90df
[6] S. Erfantalab, et al., "Determination of thermal conductivity, thermal diffusivity and specific heat capacity of porous silicon thin films using the 3ω method," *International Journal of Heat and Mass Transfer*, vol. 184, 122346, 2022. DOI: 10.1016/j.ijheatmasstransfer.2021.122346
[7] S.-J. Kweon, et al., "On-chip sinusoidal signal generators for electrical impedance spectroscopy: Methodological review," *IEEE Transactions on Biomedical Circuits and Systems*, vol. 16, no. 3, pp. 337–360, 2022. DOI: 10.1109/TBCAS.2022.3171163
[8] J. Huang, et al., "Low-noise, high-linearity sine-wave generation using noise-shaping phase-switching technique," *IEEE Transactions on Instrumentation and Measurement*, vol. 71, pp. 1–7, 2021. DOI: 10.1109/TIM.2021.3139662
[9] I. V. Lam, "Analysis of improved Howland current pump configurations," Texas Instruments, 2023. [Online]. Available: https://www.ti.com/lit/an/sboa437a/sboa437a.pdf [Accessed: Aug. 31, 2025].
[10] I. Chaltakov, "Design of a sine-wave constant current source switching power supply for laser applications," *Journal of Physics E: Scientific Instruments*, vol. 21, no. 7, p. 663, 1988. DOI: 10.1088/0022-3735/21/7/008
[11] S. Abbas, et al., "Constant current AC source using Improved Howland Pump for exciting eddy current testing (ECT) probe," in *Proc. 17th IEEE International Multi Topic Conference (INMIC)*, 2014, pp. 508–513, DOI: 10.1109/INMIC.2014.7097393
[12] N. Ahmed, et al., "Microcontroller based pure sine wave inverter," in *Proc. IEEE Int. Conf. in Power Engineering Application (ICPEA)*, 2021, pp. 173–177. DOI: 10.1109/ICPEA51500.2021.9417841
[13] D. S. Batista, et al., "Analysis and practical implementation of a high-power Howland Current Source," *Measurement*, vol. 207, p. 112404, 2023. DOI: 10.1016/j.measurement.2022.112404
[14] G. Jintao and P. Sanbo, "Simulation and design of DAC based on R2R resistor network," in *Proc. SPIE 13657, Second Int. Conf. on Power Electronics and Artificial Intelligence (PEAI)*, 2025, p. 1365718. DOI: 10.1117/12.3066830
[15] H. Chen and C. Lou, "Bridging digital and analog worlds: A comprehensive introduction of DACs," in *AIP Conference Proceedings*, vol. 3194, no. 1, p. 040002, 2024. DOI: 10.1063/5.0222538
[16] A. Suksawad, et al., "Design and practice of simple first-order all-pass filters using commercially available IC and their applications," *EUREKA: Physics and Engineering*, no. 3, pp. 40–56, 2022. DOI: 10.21303/2461-4262.2022.002416
[17] Y. Wang, et al., "A comprehensive investigation on the selection of high-pass harmonic filters," *IEEE Transactions on Power Delivery*, vol. 37, no. 5, pp. 4212–4226, 2022. DOI: 10.1109/TPWRD.2022.3147835
[18] U. Dema, et al., "Design of FM Transmitter and Receiver Operating in the Range of 88 MHz To 108 MHz," *Zorig Melong: A Technical Journal of Science, Engineering and Technology*, vol. 5, no. 1, pp. 56–60, 2021. DOI: 10.17102/zmv5.i1.011
[19] C. Mangelsdorf, "Who's afraid of positive feedback? [Shop Talk: What you didn't Learn in School]," *IEEE Solid-State Circuits Magazine*, vol. 16, no. 3, pp. 19–26, 2024. DOI: 10.1109/MSSC.2024.3419594
[20] Y.-H. Wang, et al., "MEMS-based gas flow sensors," *Microfluidics and Nanofluidics*, vol. 6, no. 3, pp. 333–346, 2009. DOI: 10.1007/s10404-008-0383-4
[21] Z. Jie, "Research of High Precision Frequency Measure Algorithm Based on LabVIEW," in *Proc. 8th Int. Conf. on Electronic Measurement and Instruments (ICEMI)*, 2007, pp. 3–268-3-271. DOI: 10.1109/ICEMI.2007.4350906
[22] S. Kommandur, et al., "A microbridge heater for low power gas sensing based on the 3-Omega technique," *Sensors and Actuators A: Physical*, vol. 233, pp. 231–238, 2015. DOI: 10.1016/j.sna.2015.07.011

УДК 621.382

Є. О. Гребьонкін
Національний технічний університет України «Київський політехнічний інститут імені Ігоря Сікорського», Київ, Україна

СТАБІЛІЗОВАНЕ ЗА АМПЛІТУДОЮ ДЖЕРЕЛО ГАРМОНІЙНОГО СТРУМУ ДЛЯ МЕМС МІКРОНАГРІВАЧІВ ІЗ ЗАЗЕМЛЕНИМ НАВАНТАЖЕННЯМ

У статті представлено проєктування та експериментальну перевірку багатокаскадного джерела змінного струму зі стабілізацією амплітуди, спеціально призначеного для роботи з мікронагрівачами із заземленим навантаженням у вимірюваннях теплофізичних характеристик газів методом 3ї гармоніки.
Запропонована система побудована на основі мікроконтролера Raspberry Pi Pico, зовнішнього ЦАП на резистивній драбині, інвертуючих каскадів підсилення та покращеного джерела струму Хоуленда, що забезпечує точну стабілізацію амплітуди збуджувального струму. Такий підхід дозволяє генерувати спектрально чистий синусоїдальний сигнал у діапазоні частот 20 Гц – 20 кГц, із можливістю регулювання амплітуди струму до 5 мА, контролем нульового зсуву, підтримуючи роботу з системами типу «нагрівач-послідовний резистор» із опором від 50 Ω до 3 кΩ. Порівняно з традиційними схемами збудження напругою, струмове збудження в методі 3-омега забезпечує вищу відтворюваність, кращу стабільність калібрування та точніший аналіз теплових відгуків.
Розроблене джерело є компактною та економічною альтернативою громіздкому лабораторному обладнанню, дозволяючи проводити як вимірювання на фіксованій частоті, так і у широкому діапазоні частот.
Експериментальні результати засвідчують, що джерело струму забезпечує стабільність частоти на рівні понад 99,9 % та коєфіцієнт гармонічних спотворень нижче 1 %, при цьому відхилення амплітуди струму в межах підтримуваного діапазону навантажень не перевищують 1 %, що підтверджує можливість його застосування як джерела сигналу для МЕМС нагрівачів для визначення теплофізичних характеристик газового середовища. Значущість цієї роботи полягає не лише у практичній реалізації надійного джерела струму, а й у його потенціалі підтримувати інтеграцію МЕМС-газових сенсорів у портативні та вбудовані системи.
Модульна архітектура та генерація сигналу під контролем програмного забезпечення дозволяють легко налаштовувати систему та впроваджувати майбутні вдосконалення, зокрема впровадження цифрового зворотного зв’язку, використання прецизійних резисторних збірок або живлення від джерела однополярного струму. Загалом, розроблене джерело струму є цінним і гнучким інструментом для використання у тепловому аналізі газів, що становить вагомий крок до мініатюризації та доступності систем аналізу газів.
Keywords: bell prover; volume reproduction error; control system; mathematical model; gas parameters.

Надійшла до редакції
03 вересня 2025 року

Рецензовано
12 жовтня 2025 року